Striking influence of chain structure of polyethylene on the formation of cup-stacked carbon nanotubes/carbon nanofibers under the combined catalysis of CuBr and NiO

Jiang Gong [a,b], Jie Liu [a], Zhiwei Jiang [a,b], Jingdong Feng [a], Xuecheng Chen [a,c], Lu Wang [a,b], Ewa Mijowska [c], Xin Wen [a], Tao Tang [a,*]

[a] State Key Laboratory of Polymer Physics and Chemistry, Changchun Institute of Applied Chemistry, Chinese Academy of Sciences, Changchun 130022, China
[b] University of Chinese Academy of Sciences, Beijing 100039, China
[c] Institute of Chemical and Environment Engineering, West Pomeranian University of Technology, Szczecinul. Pulaskiego 10, 70-322 Szczecin, Poland

ARTICLE INFO

ABSTRACT

A one-pot approach was used to convert polyethylene (PE) with different chain structures into carbon nanomaterials (CNMs) under the combined catalysis of CuBr and NiO at 700 °C, including linear low density polyethylene (LLDPE), low density polyethylene (LDPE) and high density polyethylene (HDPE). The effect of chain structure of PE on the yield, morphology, microstructure, phase structure and thermal stability of CNMs, including cup-stacked carbon nanotubes (CS-CNTs) and carbon nanofibers (CNFs), were investigated by scanning electron microscope, transmission electron microscope (TEM), high-resolution TEM, X-ray diffraction, Raman spectroscopy and thermal gravimetric analysis. In addition, the degradation products from different chain structures of PE under the catalysis of CuBr were analyzed by gas chromatography and gas chromatography–mass spectrometry. It was demonstrated that the branched structure played an important effect in the degradation products of PE. The dehydrogenation and aromatization of LLDPE were remarkably promoted by Br radicals from the decomposition of CuBr to form a large amount of light hydrocarbons and a relatively small amount of aromatics, favoring the formation of long and straight CS-CNTs. However, the degradation of LDPE was not obviously influenced by Br radicals due to its high extent of branched structure, while the random cleavage of HDPE was accelerated with the formation of a lot of olefins with long chains, resulting in the formation of short and winding CNFs. This work will contribute to the conversion of mixed waste polyolefin into high value-added CNMs.
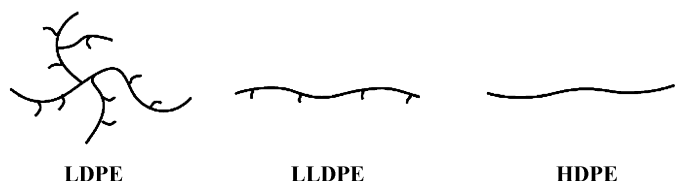
1. Introduction

Considerable attention has been paid to the treatment of waste plastics with ever-growing plastic production and consumption [1–5]. Nowadays, waste plastics are treated predominantly by landfill, incineration, mechanical recycling and chemical recycling. Landfill and incineration are far from being widely accepted by the population because of their related pollution problems. Likewise, mechanical recycling of waste plastics is limited by the low quality of the recycled plastic mixture. Chemical recycling has the advantage of recovering the petrochemical components of waste plastics, which can be used to re-manufacture plastic or to make other synthetic chemicals [6–13]. Nevertheless, a great deal of effort has been made to explore a new technically and economically feasible chemical recycling process for waste plastics.

Among waste plastics, waste polyolefin is the main component and the content of carbon in polyolefin is about 85.7 wt%. Hence, reutilization of waste polyolefin to synthesize high value-added carbon nanomaterials (CNMs) provides a novel way to recycle waste plastics. Generally complex degradation reactions occur during the conversion of mixed waste polyolefin into CNMs, therefore, the conversion of single component polyolefin into CNMs needs to be investigated first. Recently, extensive studies [14–30] have been conducted to convert virgin or waste polyolefin including polypropylene (PP) and polyethylene (PE) with different chain structures (such as low density polyethylene (LDPE), linear low density polyethylene (LLDPE) and high density polyethylene (HDPE), see Scheme 1) into CNMs with varied morphologies, such as carbon nanotubes (CNTs), carbon nanofibers (CNFs) and carbon spheres (CSs). For example, Wu et al. used catalytic gasification to convert waste PP into

Scheme 1. Typical chain structure of three commercial PE: LDPE has many long and short branched chains, LLDPE has a significant number of short branches with linear structure and HDPE has few or no branched structures.

high-quality CNTs with high yielded hydrogen-rich synthetic gas [14]. Kong et al. synthesized straight and helical CNTs and Fe_3O_4@C composite through catalytic decomposition of PE in autoclave [15,16]. Zhuo et al. reported the synthesis of CNTs and CNFs from recycled HDPE using a novel pyrolysis–combustion technique [17,18]. Pol et al. used autoclave as reactor to convert waste LDPE and HDPE into CNTs and CSs, which showed high performances in lithium electrochemical cells [19,20]. Our group has put forward a strategy of "combined catalysts", that is, degradation catalyst/carbonization catalyst, including solid acids (such as organically-modified montmorillonite or zeolite)/nickel catalysts [21–24], halogenated compounds/Ni_2O_3 [25,26] and activated carbon/Ni_2O_3 [27] to convert polyolefin into CNTs, cup-stacked CNTs (CS-CNTs), CNFs and CSs [28].

Unfortunately, although many investigations have been conducted to convert PE into CNMs with diverse morphologies, there are no investigations about the effect of chain structure of PE on the formation of CNMs. This is very important to convert mixed waste polyolefin into CNMs because PE is the main component in mixed waste polyolefin, and the sum content of PE and PP accounts entirely for roughly 60% of the whole waste plastics [5,31]. Furthermore, in the combined halogenated compounds/Ni_2O_3 catalysts [26], it was found that halogenated radicals from the decomposition of halogenated compounds affected the degradation products of LLDPE by promoting the dehydrogenation and aromatization of LLDPE macroradical fragments, which finally played a crucial role in the yield and morphology of CNMs. The previous work prompted us to raise further questions: How does the chain structure of PE (see Scheme 1) influence the yield, morphology and microstructure of CNMs? How do halogenated radicals affect the degradation products from different chain structures of PE? Solving these problems will not only favor to control the degradation of mixed waste polyolefin, but also help to convert mixed waste polyolefin into high value-added CNMs.

In this work, three commercial PE with different chain structures, including LLDPE, LDPE and HDPE, were selected as carbon sources to prepare CNMs via a one-pot approach by the combined catalysts of CuBr and nickel oxide (NiO) at 700 °C. The effect of chain structure of PE on the yield, morphology, microstructure, phase structure and thermal stability of the resultant CNMs (including CS-CNTs and CNFs) were investigated. In addition, the effect of chain structure on the degradation products of PE under the catalysis of CuBr was analyzed. It is believed that this work will contribute to the conversion of mixed waste polyolefin into high value-added CNMs.

2. Experimental part

2.1. Materials

Linear low density polyethylene (LLDPE, trademark DFDA-7042, $M_w = 1.41 \times 10^4$ g/mol and polydispersity = 3.36) and low density polyethylene (LDPE, trademark 951-050, $M_w = 1.89 \times 10^4$ g/mol and polydispersity = 7.84) were supplied by Sinopec Maoming Company. High density polyethylene (HDPE, trademark 5306J,

$M_w = 1.53 \times 10^4$ g/mol and polydispersity = 5.55) was obtained from Sinopec Yangzi Petrochemical Co., Ltd. Nano-sized nickel oxide (NiO) was prepared by sol–gel combustion synthesis method. Precursor solution was prepared as following: 29.08 g $Ni(NO_3)_2 \cdot 6H_2O$ and 5.76 g citric acid were dissolved in 200 ml ethanol. The resultant solution was evaporated at 80 °C to forming gel, which was further heated in air up to the temperature of self-ignition. Upon ignition, the obtained NiO was used as carbonization catalyst for synthesizing CNMs. Cuprous bromide (CuBr, purchased from Beijing Chemical Works) was of analytical grade and used without further purification. All of the chemicals were of analytical-grade quality.

2.2. Preparation of samples

LLDPE, LDPE or HDPE (40.00 g) was mixed with NiO (3.00 g) and a designed amount of CuBr in a Brabender mixer at 100 rpm and 160 °C for 8 min. The resultant samples were denoted as LLDPE/CuBr-NiO-x, LDPE/CuBr-NiO-x or HDPE/CuBr-NiO-x, respectively, where x represented the content of CuBr in the mixture. For comparison, LLDPE/NiO, LDPE/NiO and HDPE/NiO with NiO content of 7.5 (g/100 g PE), and LLDPE/CuBr-x, LDPE/CuBr-x and HDPE/CuBr-x mixtures were also prepared.

2.3. Preparation of CNMs

CNMs were prepared according to our previous report [25]. Briefly, a piece of sample (about 5.0 g) was placed into a crucible, which was heated at 700 °C until the flame from the crucible's upper brim went out. Subsequently, the obtained CNMs were cooled to room temperature and designated as CNM-LL-x, CNM-L-x and CNM-H-x, which represented CNMs from LLDPE/CuBr-NiO-x, LDPE/CuBr-NiO-x and HDPE/CuBr-NiO-x, respectively. The yield of CNMs was calculated by dividing the amount of the obtained carbon (the amount of the residue after subtracting the amount of the residual catalysts) by that of carbon element in the sample. Each measurement was repeated four times for reproducibility purpose.

The degradation products of LLDPE, LDPE or HDPE are carbon feedstock for the formation of CNMs. In order to study the effect of chain structure on the degradation products of PE under the catalysis of CuBr, pyrolysis experiments based on our previous report [25] for LLDPE, LLDPE/CuBr-0.1, LDPE, LDPE/CuBr-0.1, HDPE and HDPE/CuBr-0.1 were conducted at 700 °C in a fixed bed reactor as model experiments. The quartz tube with a crucible in the middle was vertically mounted in an electrical resistance furnace and heated to 700 °C under N_2 atmosphere (N_2 was used to blow off the air in the tube before pyrolysis and the degraded products after pyrolysis). Subsequently, a sample (~2.5 g) was put into the crucible and pyrolyzed at 700 °C. The liquid products were collected using a cold trap and the gas products were collected using a sample bag.

2.4. Characterization

The morphologies of NiO and CNMs were observed by means of field-emission scanning electron microscope (SEM, XL30ESEM-FEG). The microstructures of NiO and CNMs were investigated using transmission electron microscope (TEM, JEM-1011) at an accelerating voltage of 100 kV and high-resolution TEM (HRTEM) performed on a FEI Tecnai G2 S-Twin transmission electron microscope operating at 200 kV. The phase structures of NiO and CNMs were analyzed by X-ray diffraction (XRD) using a D8 advance X-ray diffractometer with Cu Kα radiation operating at 40 kV and 200 mA. The vibrational property of CNMs was characterized by Raman spectroscopy (T6400, excitation-beam wavelength: 514.5 nm). The thermal stability of CNMs was measured by thermal gravimetric analysis (TGA)
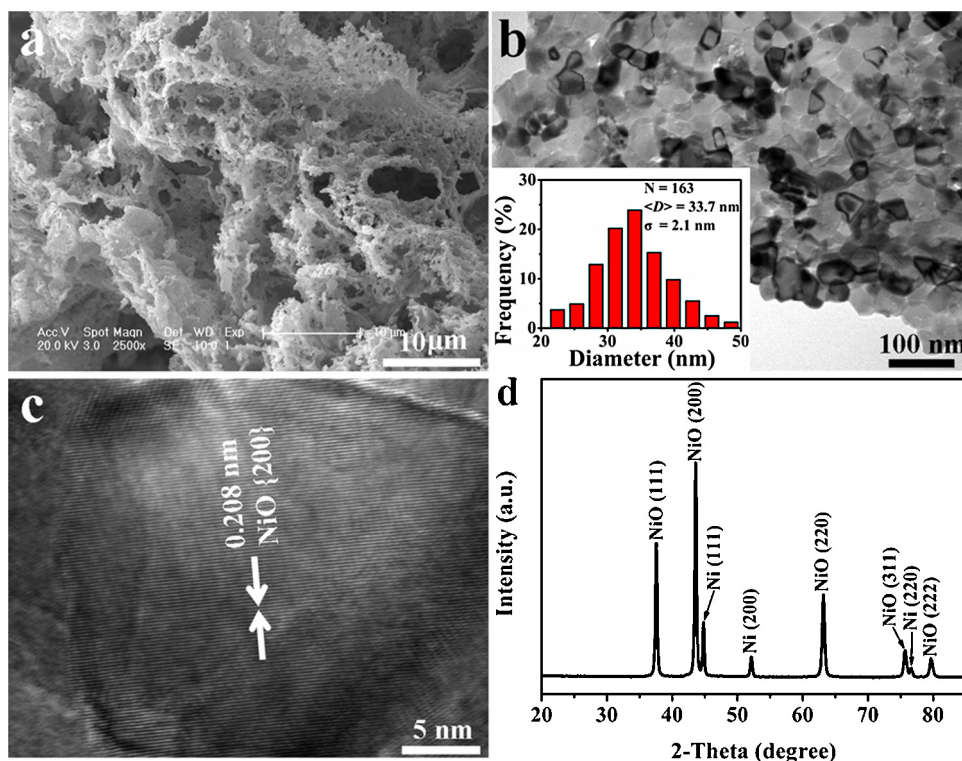
Fig. 1. Characterization of the obtained NiO catalyst from sol–gel combustion synthesis method by SEM (a), TEM (b), HRTEM (c) and XRD (d). The inset image shows the size distribution histogram of NiO nanoparticles.

under air flow at a heating rate of 10 °C/min using a TA Instruments SDT Q600. The liquid degradation products from LLDPE, LLDPE/CuBr-0.1, LDPE, LDPE/CuBr-0.1, HDPE and HDPE/CuBr-0.1 at 700 °C were weighed and analyzed by gas chromatography-mass spectrometry (GC-MS, AGILENT 5975MSD). The volume of gas degradation products was determined by the displacement of water. The hydrocarbon gas products were analyzed by a GC (Kechuang, GC 9800) equipped with a FID, using a KB-Al$_2$O$_3$/Na$_2$SO$_4$ column (50 m × 0.53 mm ID). H$_2$, CO and CH$_4$ were analyzed by a GC (Kechuang, GC 9800) equipped with a TCD, using a packed TDX-01 (1 m) and molecular sieve 5A column (1.5 m).

3. Results and discussion

3.1. Characterization of NiO catalyst

The NiO catalyst was synthesized via sol–gel combustion using ethanol as solution. As shown in Fig. 1a, SEM image showed that the obtained NiO catalyst was foam lamellar structure ranging from hundreds of nanometers to several micrometers in length. The corresponding TEM image is shown in Fig. 1b, demonstrating that the resultant NiO catalyst consisted of uniform NiO nanoparticles with a mean diameter of 33.7 nm as depicted in the size distribution histogram (the inset image in Fig. 2b). The HRTEM image of typical NiO nanoparticles (Fig. 1c) showed that there were distinct lattice patterns, indicating that the NiO nanoparticles were well crystallized. The typical interplanar distance of about 0.208 nm could be indexed to the {2 0 0} plane of NiO. The XRD pattern of NiO catalyst is shown in Fig. 1d. Characteristic diffraction peaks were observed at $2\theta = 37.6$, 43.6, 63.2, 75.7 and 79.7°, which corresponded to the (1 1 1), (2 0 0), (2 2 0), (3 1 1) and (2 2 2) reflections of NiO, respectively, consistent with HRTEM observation (Fig. 1c). The size of NiO nanoparticles calculated from the (200) reflection using Scherrer's formula was 28.3 nm, which well matched with TEM observation

(Fig. 1b). In addition, characteristic diffraction peaks of metallic nickel were observed at $2\theta = 44.8°$ (1 1 1), 52.1° (2 0 0) and 76.6° (2 2 0), indicating the existence of metallic nickel in the obtained NiO catalyst. This is ascribed to the reduction of NiO by the decomposition products of gel such as H$_2$ and CH$_4$ [32].

3.2. Effect of chain structure of PE on the yield of CNMs

Fig. 2 shows the effect of chain structure of PE on the yield of CNMs from PE/CuBr-NiO-x mixtures at 700 °C. In the cases of PE/NiO (including LLDPE/NiO, LDPE/NiO and HDPE/NiO) or PE/CuBr-x (including LLDPE/CuBr-x, LDPE/CuBr-x and HDPE/CuBr-x), the yield of CNMs was less than 7.5 or 1.0 wt%, respectively, indicating that NiO or CuBr alone could not effectively catalyze
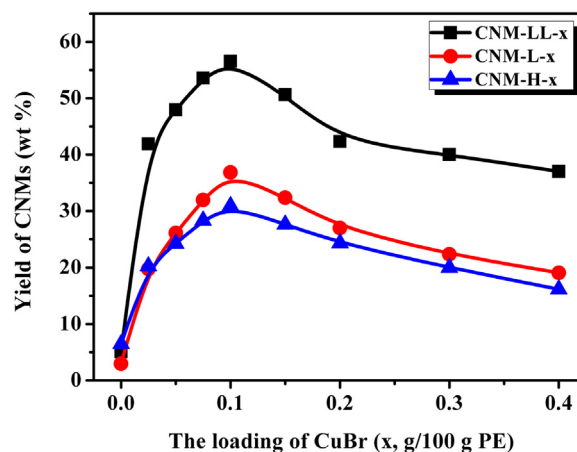

Fig. 2. Effect of chain structure of PE on the yield of CNMs from PE/CuBr-NiO-x mixtures at 700 °C.
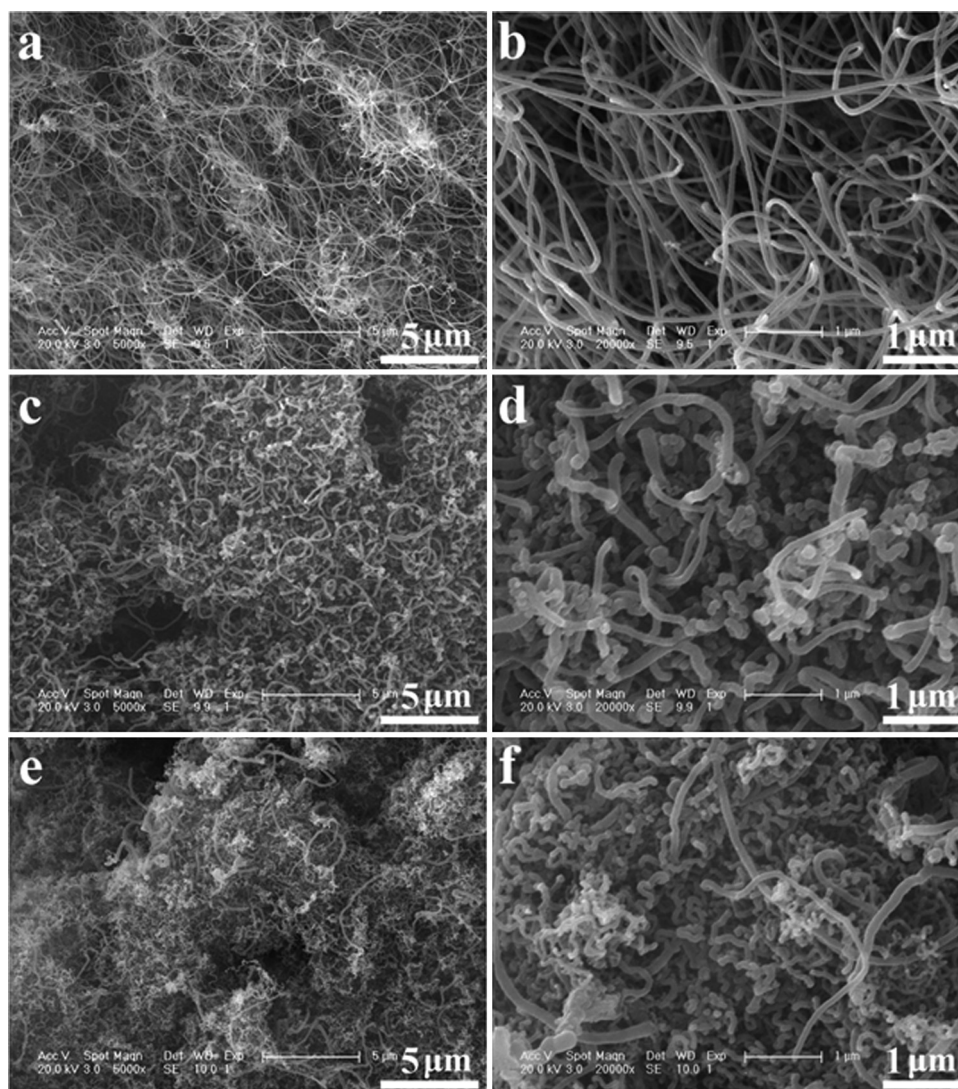
Fig. 3. Typical SEM images of CNM-LL-0.1 from LLDPE/CuBr-NiO-0.1 mixture (a and b), CNM-L-0.1 from LDPE/CuBr-NiO-0.1 mixture (c and d) and CNM-H-0.1 from HDPE/CuBr-NiO-0.1 mixture (e and f) at 700 °C.

carbonization of PE. Interestingly, regardless of the chain structure of PE, the variation for the yield of CNMs showed similar trends after adding CuBr into PE/NiO mixture, that is, the yield of CNMs dramatically increased at first, reached the maximum value and subsequently decreased with further increasing the content of CuBr. Hence the combination of NiO with CuBr showed a synergetic effect on the carbonization of PE into CNMs.

Taking LLDPE as an example, the yield of CNMs increased from 5.1 to 41.9 wt% after adding 0.025 g CuBr (/100 g LLDPE) into LLDPE/NiO mixture, reached the maximum value of 56.5 wt% after adding 0.1 g CuBr (/100 g LLDPE) and finally decreased with further increasing the amount of CuBr. The yield of CNMs reached the maximum value of 36.8 wt% for LDPE/CuBr-NiO-x mixtures and 30.9 wt% for HDPE/CuBr-NiO-x mixtures. As can be seen from Fig. 2, the yield of CNM-LL-x was much higher than that of CNM-L-x or CNM-H-x, suggesting that the chain structure of PE strongly affected the yield of CNMs under the combined catalysis of CuBr and NiO. Since the degradation products of PE are carbon feedstock for the formation of CNMs, different chain structures of PE produce different degradation products, which thus affect the yield of CNMs. More investigations about the degradation products from different chain structures of PE and their influence on the yield of CNMs were conducted in the latter Section 3.5.

3.3. Effect of chain structure of PE on the morphology and microstructure of CNMs

To investigate whether the chain structure of PE had any effects on the morphology and microstructure of CNMs, SEM, TEM and HRTEM observations were performed for the resultant CNMs from LLDPE/CuBr-NiO-0.1, LDPE/CuBr-NiO-0.1 and HDPE/CuBr–NiO-0.1 mixtures at 700 °C. Fig. 3 shows the typical SEM images of the resultant CNMs. Strikingly, when LLDPE was used as carbon source, there were a great amount of relatively straight and long filamentous carbon in the obtained CNM-LL-0.1 (Fig. 3a and b). However, in the case using LDPE or HDPE as carbon source, the resultant CNM-L-0.1 or CNM-H-0.1 mainly consisted of short and winding filamentous carbon (Fig. 3c–f). Fig. 4 displays the typical TEM images of the corresponding CNMs. It was observed that the resultant relatively straight and long filamentous carbon from CNM-LL-0.1 had a tubular-like form (Fig. 4a and 4b), which is characteristic of CNT. The surface of CNTs seemed to be smooth and they had narrow diameter and length distributions. The mean outer diameter and length were 92.0 nm and 8.5 μm, respectively. Interestingly, most of the metallic nickel catalysts were found to be rhombic and embedded in the middle of long, straight and smooth-surface CNTs (Fig. 4a, marked using white dashed circles), similar with our
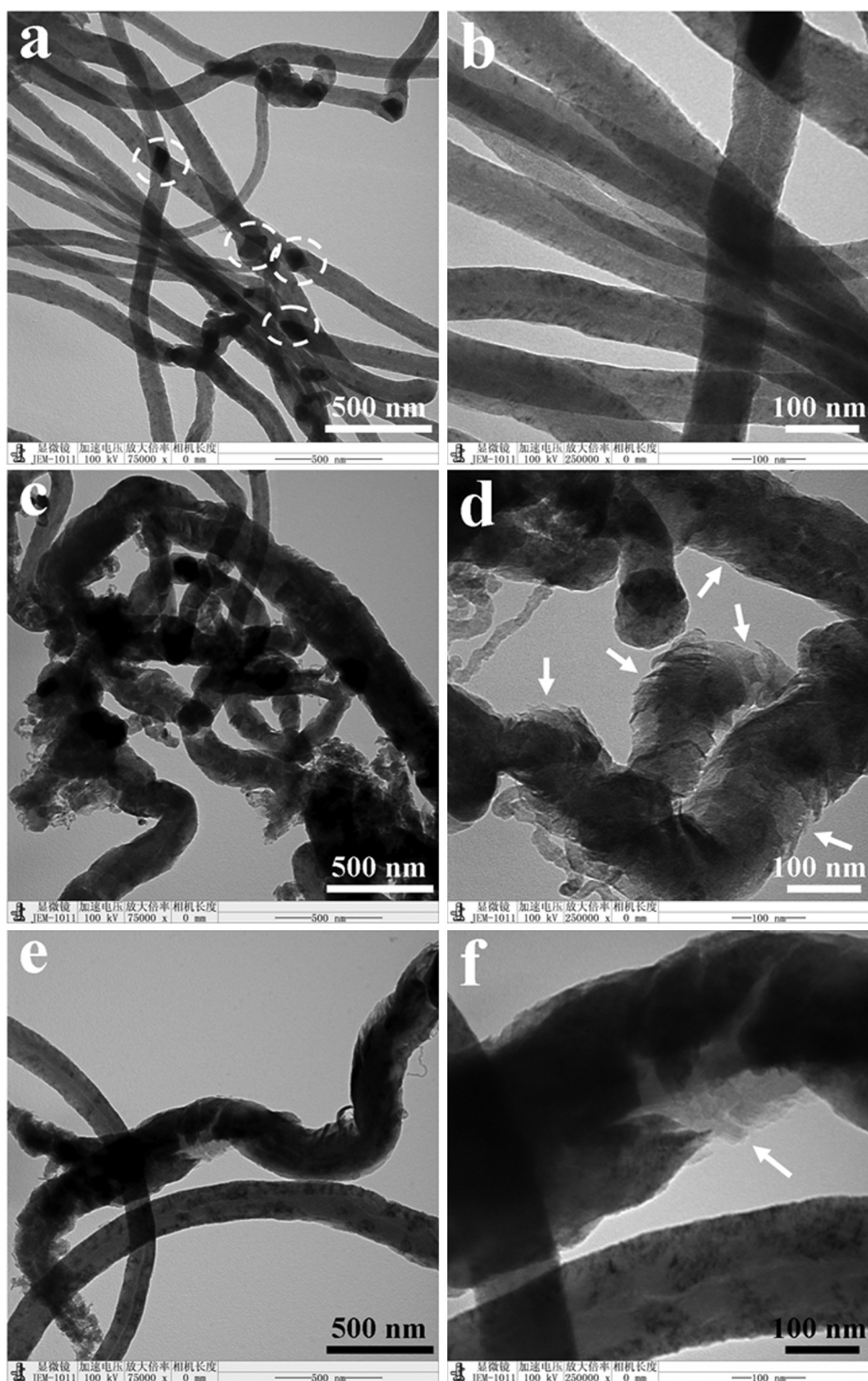
Fig. 4. Typical TEM images of CNM-LL-0.1 from LLDPE/CuBr-NiO-0.1 mixture (a and b), CNM-L-0.1 from LDPE/CuBr-NiO-0.1 mixture (c and d) and CNM-H-0.1 from HDPE/CuBr-NiO-0.1 mixture (e and f) at 700 °C.

previous work [24]. Comparatively, short, winding and surface-rugged CNFs with wide diameter and length distributions were found in both CNM-L-0.1 and CNM-H-0.1 (Fig. 4c–f). The main diameter and length of CNFs were in the ranges of 50–200 nm and 500 nm to several micrometers, respectively.

To further clarify the effect of chain structure of PE on the microstructure of the resultant CNTs and CNFs, HRTEM

observations were conducted on the CNM-LL-0.1 and CNM-L-0.1 as shown in Fig. 5. Surprisingly, the graphitic layers in the long, straight and smooth-surface CNTs from CNM-LL-0.1 were oblique to the CNT axis at the angle of 20–25° (Fig. 5a). On the basis of this result, the obtained CNTs are identified as CS-CNTs, which are different from conventional CNTs made up of multi-seamless cylinders of hexagonal carbon networks. As a result, a large portion of
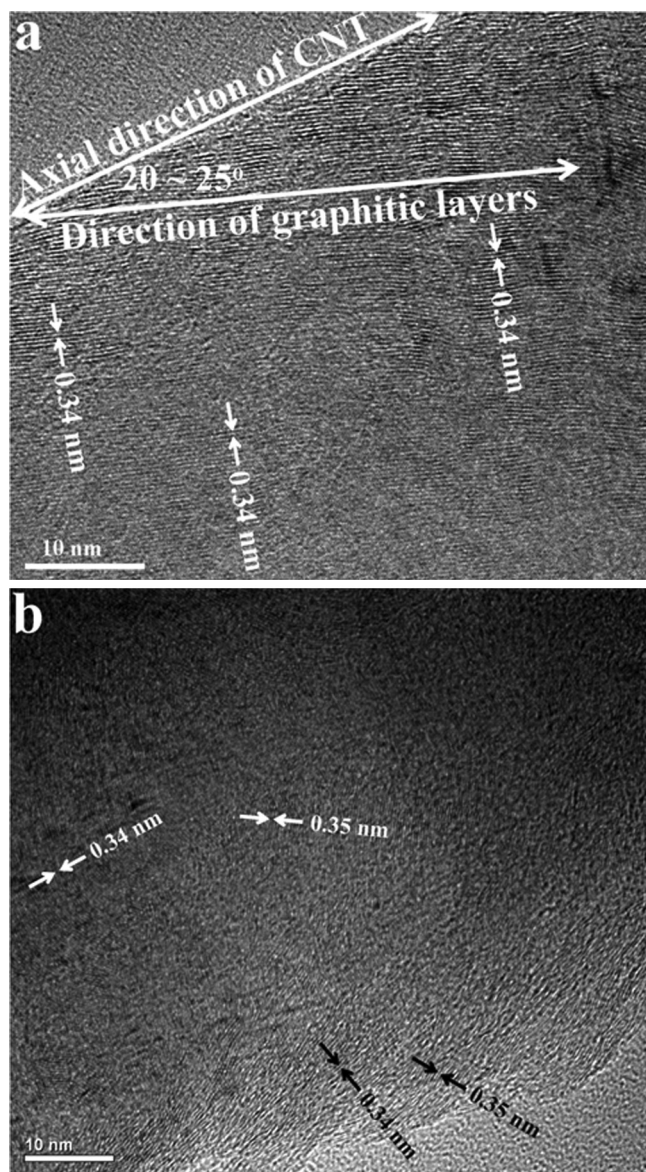
Fig. 5. Typical HRTEM images of long, straight and smooth-surface CS-CNTs in the CNM-LL-0.1 from LLDPE/CuBr-NiO-0.1 mixture (a) and short, winding and rugged-surface CNFs in the CNM-L-0.1 from LDPE/CuBr-NiO-0.1 mixture (b).

Fig. 6. XRD patterns (a), Raman spectra (b) and DTG curves (c) of CNM-LL-0.1, CNM-L-0.1 and CNM-H-0.1.

exposed and reactive edges with abundant dangling bonds exist on the outer surface and in the inner channel of CS-CNTs [33], which makes them excellent candidates in the applications of nanoelectronics [34], absorbents [35], nancomposites [36], energy [37], electrochemical biosensors [38], and heterogeneous catalysis [39], *etc.* Moreover, the interlayer spacing between graphitic layers in the resultant CS-CNTs was about 0.34 nm, which is consistent with the ideal graphitic interlayer spacing. However, the graphitic layers in the short, winding and rugged-surface CNFs from CNM-L-0.1 were random orientation to the CNF axis (Fig. 5b). The interlayer spacing between graphitic layers was in the range of 0.34–0.36 nm, suggesting the relatively low graphitization of CNFs using LDPE or HDPE as carbon source. According to the above results, a conclusion could be drawn that the chain structure of PE remarkably affected the morphology and microstructure of CNMs from the carbonization of PE under the combined catalysis of CuBr and NiO.
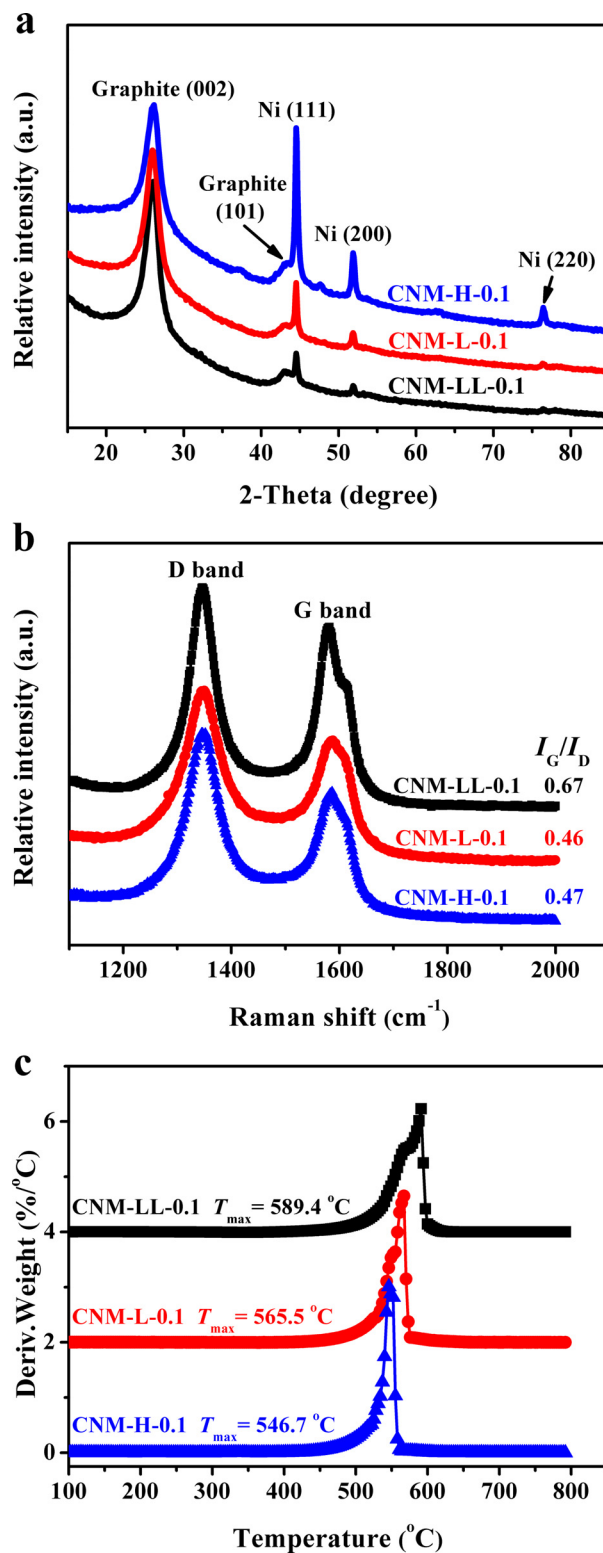
3.4. Effect of chain structure of PE on the phase structure and thermal stability of CNMs

XRD, Raman and TGA measurements were conducted to further study the effect of chain structure of PE on the phase structure and thermal stability of CNMs. Fig. 6a displays the XRD patterns of the resultant CNMs. Characteristic diffraction peaks of both graphite

$(2\theta = 26.2°$ and $42.9°)$ and metallic Ni $(2\theta = 44.5°$, $51.9°$ and $76.5°)$ were observed. This indicated that NiO was reduced into metallic nickel, which was the real catalyst for the growth of CS-CNTs or CNFs. Furthermore, the intensity ratio of diffraction peak of graphite (0 0 2) to that of metallic nickel (1 1 1) in CNM-LL-0.1 was larger than that from CNM-L-0.1 or CNM-H-0.1. This suggested that the CS-CNTs in CNM-LL-0.1 contained less lattice distortions, agreeing with the HRTEM observation (Fig. 5). Fig. 6b presents the Raman spectra of the corresponding CNMs. The peak at about 1580 cm^{-1} (G band) corresponds to an E_{2g} mode of hexagonal graphite and is related to the vibration of sp^2-bonded carbon atoms in a graphite layer, and the D band at about 1350 cm^{-1} is associated with vibration of carbon atoms with dangling bonds in the plane terminations of disordered graphite or glassy carbons [40]. A larger I_G/I_D ratio indicates a higher degree of structural ordering for CNMs [41]. Obviously, CNM-LL-0.1 showed a larger I_G/I_D ratio (0.67) than CNM-L-0.1 (0.46) and CNM-H-0.1 (0.47), indicating that CNM-LL-0.1 had relatively lower defects inside the graphite sheets than CNM-L-0.1 and CNM-H-0.1. TGA was used to measure thermal stability of CNMs, which gave an overall quality of CNMs. Higher oxidation temperature is always associated with purer, less defective CNMs. Fig. 6c shows the derivative TGA (DTG) curves of the corresponding CNMs under air flow at a heating rate of 10 °C/min. The weight loss from 500 to 650 °C was due to the oxidation of CNTs or CNFs. CNM-LL-0.1 showed the maximum oxidation temperature at 589.4 °C, evidently higher than that from CNM-L-0.1 (565.5 °C) or CNM-H-0.1 (546.7 °C), revealing the formation of well graphitized CS-CNTs using LLDPE as carbon source, consistent with the results of SEM, TEM, XRD and Raman. The above results demonstrated that the chain structure of PE significantly influenced the phase structure and thermal stability of CNMs.

3.5. Effect of chain structure of PE on the formation of CNMs

The degradation products of PE are carbon sources for the formation of CS-CNTs or CNFs. In order to study the effect of chain structure of PE on the degradation products under the catalysis of CuBr, LLDPE, LLDPE/CuBr-0.1, LDPE, LDPE/CuBr-0.1, HDPE and HDPE/CuBr-0.1 were pyrolyzed at 700 °C, and subsequently GC and GC–MS measurements were conducted to analyze the composition of the degradation products. Table 1 presents the results of mass balance. The yields of gas products from PE or PE/CuBr-0.1 mixtures calculated by mass balance (the third column) were approximate to those calculated by GC measurement (the fourth column), demonstrating that the mass balance was reliable. It was evident that different chain structures of PE produced different degradation products under the catalysis of CuBr. In the case of LLDPE, the yield
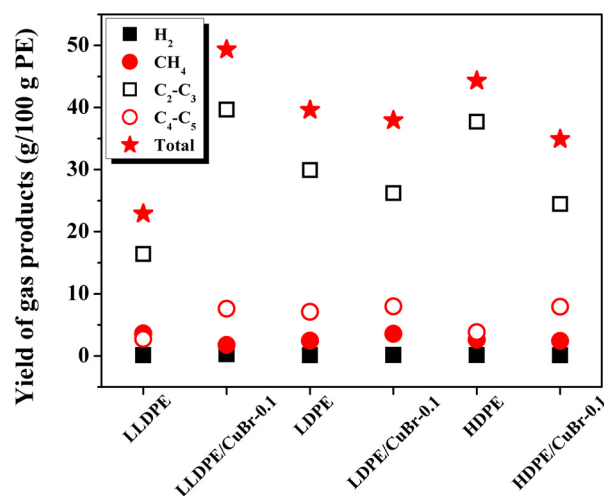

Fig. 7. Yield of gas degradation products from LLDPE, LLDPE/CuBr-0.1, LDPE, LDPE/CuBr-0.1, HDPE and HDPE/CuBr-0.1 at 700 °C.

of liquid degradation products decreased from 75.4 to 51.7 (g/100 g LLDPE) after adding 0.1 g CuBr (/100 g LLDPE), meanwhile the yield of gas degradation products increased significantly from 24.6 to 49.3 (g/100 g LLDPE). This result indicated that a small amount of CuBr could efficiently promote the dehydrogenation of LLDPE into light hydrocarbons. In contrast, the yields of both liquid and gas degradation products from LDPE did not show obvious changes after adding 0.1 g CuBr (/100 g LDPE). But the yield of liquid degradation products from HDPE increased from 58.3 to 63.6 (g/100 g HDPE) after adding 0.1 g CuBr (/100 g HDPE), meanwhile the yield of gas degradation products decreased from 41.7 to 36.4 (g/100 g HDPE).

Fig. 7 and Table S1 show the composition of gas degradation products from the above samples in details. The gas degradation products mainly consisted of hydrogen, methane, ethane, ethylene, propane, propylene and *i*-butene. Compared to LLDPE, the yield of C$_2$–C$_3$ gas fraction products increased from 16.4 to 39.7 (g/100 g LLDPE) after adding 0.1 g CuBr (/100 g LLDPE). However, the yield of gas degradation products from LDPE did not show obvious changes, and the yield of C$_2$–C$_3$ gas fraction products from HDPE decreased from 37.7 to 24.5 (g/100 g HDPE) after adding 0.1 g CuBr (/100 g HDPE). Since the C$_2$–C$_3$ gas fraction products are good carbon sources for the growth of CNTs [42,43], the relatively high yield of C$_2$–C$_3$ gas fraction products from LLDPE/CuBr-0.1 is favorable to the formation of CS-CNTs. This is a reason for the high yield of CS-CNTs from LLDPE/CuBr-NiO-0.1 mixture.

Fig. 8 displays the GC–MS profiles of liquid degradation products from LLDPE, LLDPE/CuBr-0.1, LDPE, LDPE/CuBr-0.1, HDPE and HDPE/CuBr-0.1 at 700 °C. Table S2 presents the main composition of liquid degradation products. The liquid degradation products consisted of olefins with long chains, aromatics (such as benzene and toluene) and alkanes. After adding 0.1 g CuBr (/100 g PE), the content of aromatics increased from 10.6 to 12.1 (area %) for LLDPE or 13.8 to 18.1 (area %) for LDPE, but decreased from 26.2 to 14.5 (area %) for HDPE. Meanwhile, the content of olefins with long chains decreased from 79.2 to 78.0 (area %) for LLDPE or 75.8 to 74.9 (area %) for LDPE, but increased from 67.5 to 77.1 (area %) for HDPE.

Hence the chain structure had an important influence in the degradation of PE under the catalysis of CuBr. A relatively large amount of light hydrocarbons with a certain amount of aromatics were formed from LLDPE. But the yields of both liquid and gas degradation products from LDPE did not show obvious changes, and a relatively large amount of olefins with long chains and small

Table 1
Yields of the different fractions from the degradation of LLDPE, LLDPE/CuBr-0.1, LDPE, LDPE/CuBr-0.1, HDPE and HDPE/CuBr-0.1 at 700 °C.

Sample	Liquid (g/100 g PE)	Gas[a] (g/100 g PE)	Gas[b] (g/100 g PE)	Gas[c] (mL/g PE)
LLDPE	75.4	24.6	22.9	193.8
LLDPE/CuBr-0.1	51.7	49.3	49.9	357.0
LDPE	60.9	39.1	39.6	289.1
LDPE/CuBr-0.1	61.0	39.0	37.9	258.4
HDPE	58.3	41.7	44.3	328.8
HDPE/CuBr-0.1	63.6	36.4	34.9	263.8

[a] Calculated by the mass balance.
[b] Calculated by the volume of one gas first divided by 22.4 L/mol, multiplying the molar number of the gas by its molar mass, and then obtained the yield of one gas (g/100 g PE) by dividing the mass of the gas by the mass of PE in PE/CuBr-x mixtures and finally obtained the yield of total gas products by adding the yield of one gas together.
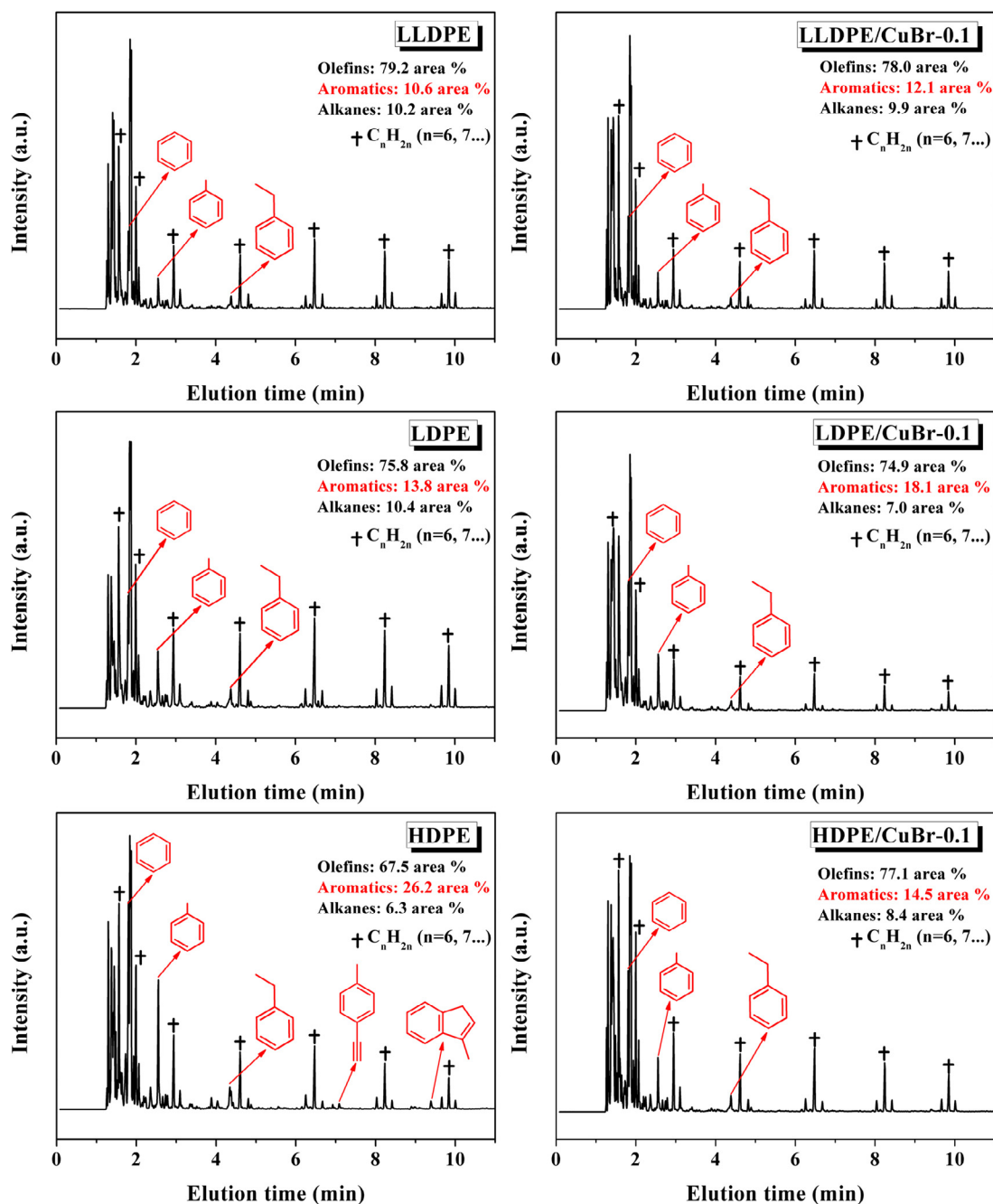[c] Calculated by the displacement of water.

Fig. 8. GC–MS profiles of liquid degradation products from LLDPE, LLDPE/CuBr-0.1, LDPE, LDPE/CuBr-0.1, HDPE and HDPE/CuBr-0.1 at 700 °C.

amounts of aromatics and gas products were formed from HDPE. It is generally accepted that thermal cracking degradation of PE occurs by a radical mechanism due to heat induction to crack C—C and C—H bonds [44,45]. End-chain scission and random cleavage of PE at any bond in the chain proceed simultaneously. Thus the striking difference of degradation products from different PE chain structures result from the different degradation processes of PE catalyzed by Br radicals.

LDPE has many long and short branched chains, and the branched sites act as the points of preferential cracking of C—C bonds [31]. Meanwhile, the cracking of C—H bonds with the formation of hydrogen radical proceeds easily, since tertiary hydrogen is more readily abstracted than secondary or primary one [46]. As a

result, the thermal degradation of LDPE takes place more rapidly than HDPE or LLDPE [47], and the random cleavage of LDPE chains occurs predominantly, leading to the formation of olefins with long chains, even in the presence of Br radicals. This is the reason why the degradation products of LDPE after adding CuBr show no obvious changes except for a slight increase content of aromatics (Figs. 7 and 8 and Table 1). The resultant long-chains olefins and aromatics result in the growth of short and winding CNFs [24,48].

Unlike to LDPE, HDPE has few or no branched structures, thus the formation of HDPE fragment radicals is not as easy as that in LDPE, and end-chain scission of HDPE occurs predominantly, resulting in the higher yield of gas products and lower yield of olefins with long chains (Figs. 7 and 8, and Table 1). Aromatics are mainly formed by

secondary reactions of oligomerization, cyclization and dehydrogenation of olefins, mainly C_3 and C_4 fractions. This is the reason for the higher yield of aromatics from HDPE than LDPE (Fig. 8 and Table S2). After adding CuBr, more cracking sites of HDPE chain occurs due to the abstraction of hydrogen radicals by Br radicals [49], accelerating the random cleavage of HDPE chain. Accordingly, the yield of olefins with long chains increases but the yields of aromatics and gas products decrease (Figs. 7 and 8, and Table 1). The conversion of olefins with long chains into CS-CNTs catalyzed by Ni is more difficult than that of light hydrocarbons or aromatics, and the olefins with long chains are more responsible for the growth of short and winding CNFs [24,48]. As a result, short and winding CNFs are produced from HDPE/CuBr-NiO-0.1 mixture. As can be seen, although the degradation mechanisms of LDPE and HDPE are definitely different, both LDPE and HDPE yield a lot of olefins with long chains and a relatively low amount of light hydrocarbons under the catalysis of CuBr. This is why the variation of the yield and type of carbon products from LDPE/CuBr-NiO mixtures are similar to those from HDPE/CuBr-NiO mixtures (Figs. 2–5).

Similar with LDPE, the abstraction of hydrogen radicals from LLDPE chain occur easily due to the existence of branched structure. The random cleavage of LLDPE proceeds favorably compared to HDPE, leading to the higher yield of olefins with long chains and lower yield of gas products and aromatics (Figs. 7 and 8, and Table 1). Since Br radicals promote the abstraction of hydrogen radicals and enhance the hydrogenation and aromatization of LLDPE fragment radicals, the yield of gas products increased significantly with a moderate increase content of aromatics (Figs. 7 and 8, and Table 1), which favors the formation of long, straight and surface-smooth CS-CNTs [24–26,48].

4. Conclusions

A one-pot approach was demonstrated to convert different chain structures of PE, including LLDPE, LDPE and HDPE, into high value-added CNMs such as CS-CNTs and CNFs under the combined catalysis of CuBr and NiO at 700 °C. With the increasing amount of CuBr, the yield of CNMs first increased and then decreased. The yield of CNMs reached the maximum value of 56.5 wt% for LLDPE/CuBr-NiO-x mixtures, 36.8 wt% for LDPE/CuBr-NiO-x mixtures and 30.9 wt% for HDPE/CuBr-NiO-x mixtures. Long, straight and surface-smooth CS-CNTs with graphitic layers oblique to CS-CNT axis at the angle of 20–25° were obtained from LLDPE/CuBr-NiO-x mixtures; but short, winding and surface-rugged CNFs were yielded from both LDPE/CuBr-NiO-x and HDPE/CuBr-NiO-x mixtures. The striking influence of chain structure of PE on the yield, morphology and microstructure of CNMs resulted from the different degradation products under the catalysis of CuBr, which was ascribed to the different extent of branched structure in PE chain. It was found that (i) Br radicals promoted the dehydrogenation and aromatization of LLDPE fragment radicals to form a relatively large amount of light hydrocarbons and a small amount of aromatics, which favored the formation of long, straight and surface-smooth CS-CNTs; (ii) the degradation of LDPE was not obviously affected by Br radicals due to its high extent of branched structure and (iii) the random cleavage of HDPE was promoted by Br radicals, and more olefins with long chains and less gas products and aromatics were formed, resulting in the formation of short, winding and surface-rugged CNFs.

Acknowledgments

Appendix A. Supplementary data

Supplementary data associated with this article can be found, in the online version, at http://dx.doi.org/10.1016/j.apcatb.2013.09.044.

References

[1] P.T. Williams, E. Slaney, Resour. Conserv. Recycl. 51 (2007) 754–769.
[2] S.M. Al-Salem, P. Lettieri, J. Baeyens, Waste Manage. 29 (2009) 2625–2643.
[3] A.K. Panda, R.K. Singh, D.K. Mishra, Renew. Sust. Energ. Rev. 14 (2010) 233–248.
[4] S.M. Al-Salem, P. Lettieri, J. Baeyens, Prog. Energy Combust. Sci. 36 (2010) 103–129.
[5] D.P. Serrano, J. Aguado, J.M. Escola, ACS Catal. 2 (2012) 1924–1941.
[6] T. Bhaskar, W.J. Hall, N.M.M. Mitan, A. Muto, P.T. Williams, Y. Sakata, Polym. Degrad. Stab. 92 (2007) 211–221.
[7] C.F. Wu, P.T. Williams, Appl. Catal. B: Environ. 90 (2009) 147–156.
[8] C.F. Wu, P.T. Williams, Appl. Catal. B: Environ. 87 (2009) 152–161.
[9] J.M. Escola, J. Aguado, D.P. Serrano, A. García, A. Peral, L. Briones, R. Calvo, E. Fernandez, Appl. Catal. B: Environ. 106 (2011) 405–415.
[10] J.M. Escola, J. Aguado, D.P. Serrano, L. Briones, J.L. Díaz de Tuesta, R. Calvo, E. Fernandez, Energy Fuel 26 (2012) 3187–3195.
[11] J. Aguado, D.P. Serrano, J.M. Escola, Ind. Eng. Chem. Res. 47 (2008) 7982–7992.
[12] A. López, I. de Marco, B.M. Caballero, M.F. Laresgoiti, A. Adrados, A. Aranzabal, Appl. Catal. B: Environ. 104 (2011) 211–219.
[13] A. López, I. de Marco, B.M. Caballero, M.F. Laresgoiti, A. Adrados, A. Torres, Waste Manage. 31 (2011) 1973–1983.
[14] C.F. Wu, Z.C. Wang, L.Z. Wang, P.T. Williams, J. Huang, RSC Adv. 2 (2012) 4045–4047.
[15] Q.H. Kong, J.H. Zhang, Polym. Degrad. Stab. 92 (2007) 2005–2010.
[16] J.H. Zhang, B. Yan, S. Wan, Q.H. Kong, Ind. Eng. Chem. Res. 52 (2013) 5708–5712.
[17] C.W. Zhuo, B. Hall, H. Richter, Y. Levendis, Carbon 48 (2010) 4024–4034.
[18] C.W. Zhuo, J.O. Alves, J.A.S. Tenorio, Y.A. Levendis, Ind. Eng. Chem. Res. 51 (2012) 2922–2930.
[19] V.G. Pol, M.M. Thackeray, Energy Environ. Sci. 4 (2011) 1904–1912.
[20] V.G. Pol, Environ. Sci. Technol. 44 (2010) 4753–4759.
[21] T. Tang, X.C. Chen, X.Y. Meng, H. Chen, Y.P. Ding, Angew. Chem. Int. Ed. 44 (2005) 1517–1520.
[22] Z.W. Jiang, R.J. Song, W.G. Bi, J. Lu, T. Tang, Carbon 45 (2007) 449–458.
[23] R.J. Song, Z.W. Jiang, W.G. Bi, W.X. Cheng, J. Lu, B.T. Huang, T. Tang, Chem. Eur. J. 13 (2007) 3234–3240.
[24] J. Gong, J. Liu, Z.W. Jiang, X. Wen, X.C. Chen, E. Mijowska, Y.H. Wang, T. Tang, Chem. Eng. J. 225 (2013) 798–808.
[25] J. Gong, J. Liu, L. Ma, X. Wen, X.C. Chen, D. Wan, H.O. Yu, Z.W. Jiang, E. Borowiak-Palen, T. Tang, Appl. Catal. B: Environ. 117–118 (2012) 185–193.
[26] J. Gong, K. Yao, J. Liu, X. Wen, X.C. Chen, Z.W. Jiang, E. Mijowska, T. Tang, Chem. Eng. J. 215–216 (2013) 339–347.
[27] J. Gong, J. Liu, D. Wan, X.C. Chen, X. Wen, E. Mijowska, Z.W. Jiang, Y.H. Wang, T. Tang, Appl. Catal. A: Gen. 449 (2012) 112–120.
[28] J. Gong, J. Liu, X.C. Chen, X. Wen, Z.W. Jiang, E. Mijowska, Y.H. Wang, T. Tang, Micropor. Mesopor. Mater. 176 (2013) 31–40.
[29] A. Bazargan, G. McKay, Chem. Eng. J. 195–196 (2012) 377–391.
[30] G.D. Ruan, Z.Z. Sun, Z.W. Peng, J.M. Tour, ACS Nano 5 (9) (2011) 7601–7607.
[31] D.P. Serrano, J. Aguado, J.M. Escola, J.M. Rodriguez, A. Peral, J. Catal. 276 (2010) 152–160.
[32] Y.W. Jiang, S.G. Yang, Z.H. Hua, H.B. Huang, Angew. Chem. Int. Ed. 121 (2009) 8681–8683.
[33] Y.A. Kim, T. Hayashi, Y. Fukai, M. Endo, T. Yanagisawa, M.S. Dresselhaus, Chem. Phys. Lett. 355 (2002) 279–284.
[34] Q.F. Liu, W.C. Ren, Z.G. Chen, L.C. Yin, F. Li, H.T. Cong, H.M. Cheng, Carbon 47 (2009) 731–736.
[35] G. Andrade-Espinosa, E. Muñoz-Sandoval, M. Terrones, M. Endo, H. Terrones, J.R. Rangel-Mendez, J. Chem. Technol. Biotechnol. 84 (2009) 519–524.
[36] T. Yokozeki, Y. Iwahori, S. Ishiwata, K. Enomoto, Compos. Sci. Technol. 69 (2009) 2268–2273.
[37] I.Y. Jang, H. Ogata, K.C. Park, S.H. Lee, J.S. Park, Y.C. Jung, Y.J. Kim, Y.A. Kim, M. Endo, J. Phys. Chem. Lett. 1 (2010) 2099–2103.
[38] S. Ko, Y. Takahashi, H. Fujita, T. Tatsuma, A. Sakoda, K. Komori, RSC Adv. 2 (2012) 1444–1449.
[39] K. Saito, M. Ohtani, S. Fukuzumi, J. Am. Chem. Soc. 128 (2006) 14216–14217.
[40] G.E. Ioannatos, X.E. Verykios, Int. J. Hydrogen Energy 35 (2010) 622–628.
[41] J.O. Alves, C.W. Zhuo, Y.A. Levendis, J.A.S. Tenório, Appl. Catal. B: Environ. 106 (2011) 433–444.
[42] J. Liu, Z.W. Jiang, H.O. Yu, T. Tang, Polym. Degrad. Stab. 96 (2011) 1711–1719.
[43] B. Hall, C.W. Zhuo, Y.A. Levendis, H. Richter, Carbon 49 (2011) 3412–3423.
[44] S. Kumar, A.K. Panda, R.K. Singh, Resour. Conserv. Recycl. 55 (2011) 893–910.

[45] J.F. Mastral, C. Berrueco, M. Gea, J. Ceamanos, Polym. Degrad. Stab. 91 (2006) 3330–3338.

[46] L.A. Wall, S.L. Madorsky, D.W. Brown, S. Straus, R. Simha, J. Am. Chem. Soc. 76 (13) (1954) 3430–3437.

[47] J.W. Park, S.C. Oh, H.P. Lee, H.T. Kim, K.O. Yoo, Polym. Degrad. Stab. 67 (2000) 535–540.

[48] N.R. Franklin, H.J. Dai, Adv. Mater. 12 (12) (2000) 890–894.

[49] H.O. Yu, Z.W. Jiang, J.W. Gilman, T. Kashiwagi, J. Liu, R.J. Song, T. Tang, Polymer 50 (2009) 6252–6258.